JACS
JOURNAL OF THE AMERICAN CHEMICAL SOCIETY
Article
pubs.acs.org/JACS

DNA Sequence-Dependent Morphological Evolution of Silver Nanoparticles and Their Optical and Hybridization Properties

Jiangjiexing Wu,[†,‡] Li Huey Tan,[‡] Kevin Hwang,[‡] Hang Xing,[‡] Peiwen Wu,[§] Wei Li,*[,†] and Yi Lu*[,‡,§]

[†]Collaborative Innovation Center of Chemical Science and Chemical Engineering (Tianjin) and Key Laboratory for Green Chemical Technology MOE, Tianjin University, Tianjin 300072, People's Republic of China

[‡]Department of Chemistry, University of Illinois at Urbana−Champaign, Urbana, Illinois 61801, United States

[§]Department of Biochemistry, University of Illinois at Urbana−Champaign, Urbana, Illinois 61801, United States

Supporting Information

ABSTRACT: A systematic investigation of the effects of different DNA sequences on the morphologies of silver nanoparticles (AgNPs) grown from Ag nanocube seeds is reported. The presence of 10-mer oligo-A, -T, and -C directed AgNPs growth from cubic seeds into edge-truncated octahedra of different truncation extents and truncated tetrahedral AgNPs, while AgNPs in the presence of oligo-G remained cubic. The shape and morphological evolution of the nanoparticle growth for each system is investigated using SEM and TEM and correlated with UV−vis absorption kinetic studies. In addition, the roles of oligo-C and oligo-G secondary structures in modulating the morphologies of AgNPs are elucidated, and the morphological evolution for each condition of AgNPs growth is proposed. The shapes were found to be highly dependent on the binding affinity of each of the bases and the DNA secondary structures, favoring the stabilization of the Ag{111} facet. The AgNPs synthesized through this method have morphologies and optical properties that can be varied by using different DNA sequences, while the DNA molecules on these AgNPs are also stable against glutathione. The AgNP functionalization can be realized in a one-step synthesis while retaining the biorecognition ability of the DNA, which allows for programmable assembly.

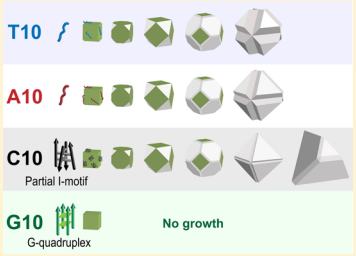

INTRODUCTION

Nanomaterial morphology, including both the shape and surface structure, plays an important role in determining the materials' physical and chemical properties. A primary example is silver nanoparticles (AgNPs),[1] whose morphologies influence many properties, including surface plasmon resonance (SPR), surface-enhanced Raman scattering (SERS), and catalytic activity.[2] For example, both SERS and localized surface plasmon resonance (LSPR) properties of Ag nanocubes with uniform edge lengths are size-dependent over the range of 30−200 nm.[2a] The Ag nanocubes also exhibited higher selectivity for heterogeneous catalysis than nanowires or nanospheres, and this enhanced selectivity is attributed to differences in the exposed Ag surface facets.[3] Changing the shape of the AgNPs from nanocubes to cuboctahedra and octahedra has also resulted in increased SERS sensitivity.[4] Recognizing the importance of controlling the morphology of AgNPs, a number of studies have been reported to demonstrate different ways to control the NPs shape. The most common method involves the use of capping agents, including dendrimers, chitosan, ionic liquids, polymers such as poly(vinylpyrrolidone) (PVP),[2e,5] and nucleic acids.[6]

Among the known types of capping agents, nucleic acids are unique; in addition to containing functional groups capable of binding metallic nanoparticles,[7] as do many other capping agents, nucleic acids are highly programmable in terms of length, charge, and sequence combination. Because of these advantages, DNA has been used as a template to position nanoparticles through DNA metallization[8] or nanoparticle attachment,[9] and such DNA-functionalized nanoparticles have been used for a variety of applications such as biosensing,[10] nanoparticle self-assembly,[9c,11] and drug delivery.[12] The majority of the work so far, however, has introduced nucleic acids only after nanomaterial synthesis, at which point DNA is unable to influence the morphology of the nanomaterial. Among the few studies that have used DNA to control the morphology of nanomaterials during their synthesis, there is evidence that different sequences of DNA can influence both the structure and function of nanomaterials, such as gold nanoparticles, silver clusters, and quantum dots.[6b,c,13] For example, DNA-directed formation of silver nanoclusters showed a photoluminescence emission band throughout the visible and near-IR range, which could be tuned by changing the oligonucleotide sequence.[13c]

To take full advantage of DNA's programmability and to provide a systematic understanding of the effects of different DNA sequences on nanomaterial morphology, we had investigated the effects of different DNA sequence combinations on the morphology of gold nanoparticles (AuNPs). We found that when the DNA molecules were incubated with nanospheres or nanoprisms as seeds, different DNA sequences had dramatic effects on the shape of surface structures on the AuNPs.[13a,b] For example, while the interaction between oligo-G

Received: June 18, 2014
Published: September 22, 2014

   dx.doi.org/10.1021/ja506150s | J. Am. Chem. Soc. 2014, 136, 15195−15202

and the Au nanoprisms caused hexagonal particle growth, interaction with oligo-T under the same conditions resulted in six-pointed star-shaped nanoparticles. More interestingly, a mixed sequence of G and T resulted in a shape partway between the hexagon and six-pointed star shapes. A transition from one shape to another was observed when different ratios of bases in the oligo were used. While these studies have established that there may be DNA "codes" for AuNPs, we wanted to find out whether such DNA "codes" might exist in other nanomaterials or with seeds of other shapes. Furthermore, it is also important to understand why different DNA sequences result in different morphologies.

In this report, we investigate the effects of different DNA sequences in modulating the morphology of AgNPs using Ag nanocubes as seeds, with L-ascorbic acid (AA) as a reductant and silver acetate (AgOAc) as the metal salt precursor. Mechanistic insight into the shape evolution with systematic variation in the DNA sequences, including the effect of the secondary structures of the DNA, was obtained through kinetic studies using UV−visible spectroscopy, transmission electron microscopy (TEM), and circular dichroism (CD). Finally, we demonstrate enhanced optical properties of AgNPs and biorecognition ability of the DNA on the synthesized nanoparticles, which may allow programmable assembly of new nanostructures with interesting properties.

RESULTS AND DISCUSSION

DNA Sequence-Dependent Control of Silver Nanoparticle Shape. To investigate the effect of different DNA sequences on the shapes and morphologies of AgNPs, we started with four different types of 10-mer DNAs consisting of either oligo-A, oligo-T, oligo-C, or oligo-G (designated as A10, T10, C10, and G10, respectively) and 40 nm Ag nanocubes coated with PVP as the seeds for nanoparticle growth. The single-crystalline silver nanocubes were prepared using a previously reported protocol.[14] These cubes, consisting of six surfaces with {100} lattice planes, are an ideal substrate to investigate the effect of DNA on AgNP growth because of the well-defined and varied facets, corners, and edges that can interact specifically with different DNA sequences and Ag^+ ion.

Images from both scanning electron microscopy (SEM) and TEM showed that the Ag nanocubes had an average particle size of ∼40 nm, with uniform distribution in terms of both shape and size (Supporting Information (SI), Figure S1). The Ag nanocubes were then incubated with 50 μM DNA for 20 min to allow adsorption of DNA onto the Ag nanocubes, followed by addition of 1.5 μL of 70 mM AA as the reductant, and 10.12 μL of 2 mM AgOAc as the source of silver in 100 μL total volume. The mixture was rigorously vortexed and left to grow for 3 h. UV−vis absorption spectra were collected from aqueous suspensions of the AgNPs. As shown in Figure S2 (SI), the AgNPs grown in the presence of A10 (designated as Ag_A10) displayed a narrow band around 480 nm, similar to the AgNPs grown in the presence of T10 (designated as Ag_T10), while AgNPs grown in the presence of C10 (Ag_C10) displayed a broad surface plasmon absorbance band around 540 nm. After growth in the presence of G10 (Ag_G10), the surface plasmon absorbance band remains unchanged from that of the initial Ag seeds. The consistent UV−vis spectra of AgNPs synthesized by this method suggest minimal batch-to-batch variation. The resulting AgNPs were visualized using TEM and SEM. Each batch of particles were uniformly shaped and monodisperse, but exhibited different morphologies depending on the DNA sequence used (Figure 1 and Figure S3 (SI)). The Ag_A10 and Ag_T10 particles

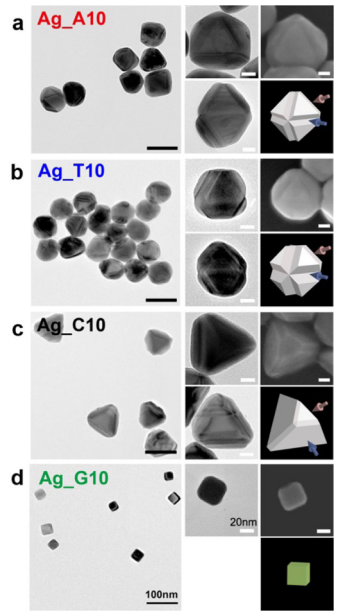

Figure 1. TEM images of AgNPs prepared in the presence of A10, T10, C10, and G10 (scale bars = 100 nm). The images to the right side of each TEM image are the TEM and SEM images of an individual nanoparticle at a higher magnification (scale bars = 20 nm; top) and corresponding 3D model (bottom). Large area views of the SEM images are available in Figure S3 (SI).

displayed an octahedral shape with edge truncation, similar to truncated stellated octahedra; the Ag_A10 were larger in size and less truncated than Ag_T10. For simplicity, these truncated stellated octahedra will be called truncated octahedra in this work. The yields of Ag_A10 and Ag_T10 are 85% and 79%, respectively, obtained from counting a total of 238 and 269 particles. The non-ideal yield is attributed to impurities from the seed solution or self-nucleation of Ag^+. Ag_C10 formed truncated tetrahedra, and Ag_G10 remained cubic after growth. Although G10 showed an apparent lack of influence on morphology, Ag_G10 particles still have a different morphology from particles grown in the absence of DNA, in which only random nanoparticle aggregates were formed (SI, Figure S4a). Furthermore, if the purified Ag nanocubes were incubated with DNA, but in the absence of a reducing agent or silver salts under otherwise identical conditions, minimal change in particle morphology was observed (SI, Figure S4b). The size distributions of AgNP_A10, Ag_T10, and Ag_C10 were found to be 82 ± 5, 74 ± 6, and 100 ± 10 nm, calculated from 82, 78, and 83 particles, respectively, from SEM and TEM micrographs (SI, Figure S5). The AgNP_C10 particles exhibited a slightly larger size distribution in comparison with the other NPs grown, corresponding well with the broader UV−vis absorbance observed (SI, Figure S2). Together these results firmly establish that it is the DNA that mediates the morphological evolution of the Ag nanocubes and that the final shape is sequence-dependent.

Kinetic Study of DNA-Directed Growth of Silver Nanoparticles. To gain a more detailed understanding of the sequence-dependent growth process, we first monitored the UV−vis absorbance changes of the AgNP growth solution in the presence of each type of DNA (Figure 2). In the presence

dx.doi.org/10.1021/ja506150s | J. Am. Chem. Soc. 2014, 136, 15195−15202

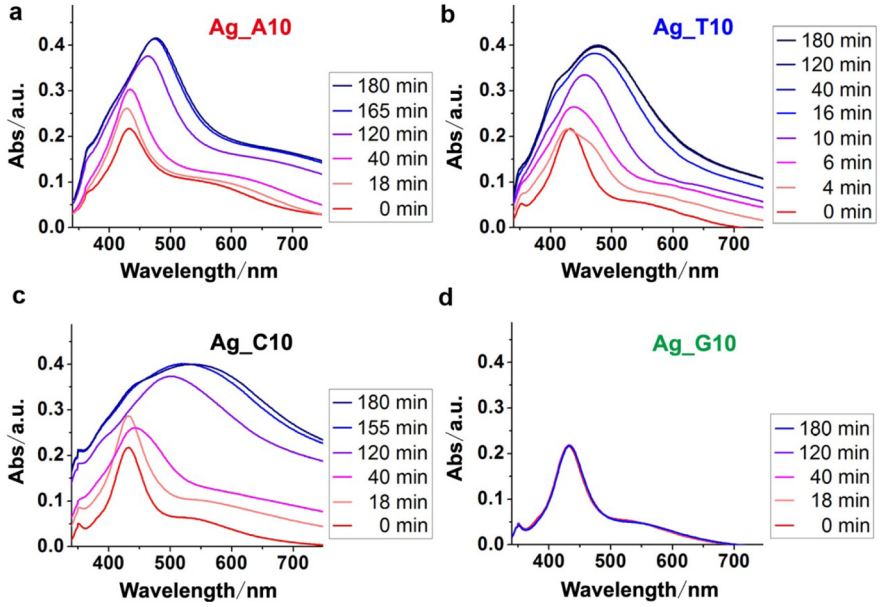

Figure 2. Time-dependent evolution of UV−vis absorption of AgNPs grown from silver nanocube seeds in the presence of (a) A10, (b) T10, (c) C10, and (d) G10.

of A10, the absorbance of the Ag nanocubes with a peak at 430 nm increased in intensity initially, blue-shifted to 424 nm in the first 18 min, and then began to red shift after 18 min and finally centered at ∼480 nm after 180 min (Figure 2a). The growth process in the presence of T10 is similar to that of A10, except that the process is faster, with the initial blue shift to 425 nm occurring in the first 4 min, followed by a red shift to 438 nm, and concluding in 40 min with a final peak at 480 nm (Figure 2b). For the growth process in the presence of C10, the absorption peak around 430 nm also increased in intensity. Instead of an initial blue shift, the peak began to red shift starting from 18 min until the end of the reaction around 180 min, in a similar time scale as Ag_A10 (Figure 2c). No absorbance change was observed in the presence of G10 (Figure 2d), consistent with SEM and TEM results that showed that G10 did not exert any effect on the morphology of the Ag nanocubes (Figure 1). These results suggest that different interactions of the DNA sequences with Ag nanocube surfaces and Ag^+ ions can lead to different pathways of shape evolution.

To gain insight into the kinetics of morphological evolution of the sequence-dependent AgNP growth in the presence of A10, T10, and C10, the morphology of the NPs at each growth stage observed from TEM images is correlated with the UV−vis absorption spectra (Figure 3 and SI, Figures S6 and S7). Particles at different stages of growth were obtained by limiting the silver precursor added to the samples where the growth was suspended due to depletion of Ag precursor. Figure 3A-a−f, shows TEM images and 3D models that illustrate the evolution of the Ag nanocube seed into truncated cubes, cuboctahedra and truncated octahedra in the presence of A10. Upon addition of 0.25 μL of 2 mM AgOAc, the cubic seeds grew into truncated cubes with {111} facets at the corner (Figure 3A-a). Increasing the quantity of AgOAc added to 1.25 μL of 2 mM AgOAc resulted in a transition from truncated cubes to Ag cuboctahedra (Figure 3A-b). Adding a total of 2.5 μL of 2 mM AgOAc caused the formation of a shape partway between octahedron and cuboctahedron (Figure 3A-c). Afterward, further increasing the amount of AgOAc added up to 10.12 μL, as used in subsequent syntheses, caused particles to grow

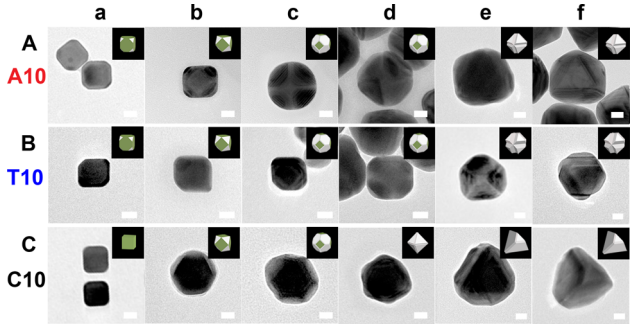

Figure 3. TEM images showing the morphological evolution of AgNPs prepared with (A) Ag_A10, (B) Ag_T10, and (C) Ag_C10. The total volume of AgOAc was 0.25 (a), 1.25 (b), 2.5 (c), 5 (d), 7.5 (e), and 10.12 μL (f), respectively. Scale bar is 20 nm. Large area view available in Figure S6 (SI). The corresponding 3D models are displayed in the top right corner of each TEM image.

into truncated octahedra with a final edge length of 82 nm (Figure 3A-d−f).

The corresponding UV−vis spectra of AgNPs grown with different amounts of AgOAc are shown in Figure S7a (SI). The wavelengths at maximum absorbance (λ_{max}) for the NPs at different growth stages of truncated cubes, cuboctahedra to truncated octahedra, show an initial blue shift to 425 nm then red shift to 440, 450, and finally 480 nm. The shift and λ_{max} values match well with the kinetic UV−vis data in Figure 2a, indicating that the shapes of the NPs observed from limiting Ag precursor are indeed representative of the intermediate shapes as the NPs grow from nanocube seeds into their final morphologies. The observation of a blue shift in λ_{max} to ∼425 nm (SI, Figure S7a) at the initial growth stages is consistent with previous reports,[15] where the corners of the cube were truncated.

The kinetics of the morphological evolution of Ag_T10 (Figure 3B-a−f and Figure S7b (SI)) are very similar to those of Ag_A10; the process also resulted in truncated octahedra, except smaller in size and containing larger crevices, with a final

dx.doi.org/10.1021/ja506150s | J. Am. Chem. Soc. 2014, 136, 15195−15202

Scheme 1. Schematic Illustration of the DNA-Mediated Shape Control of Silver Nanoparticles

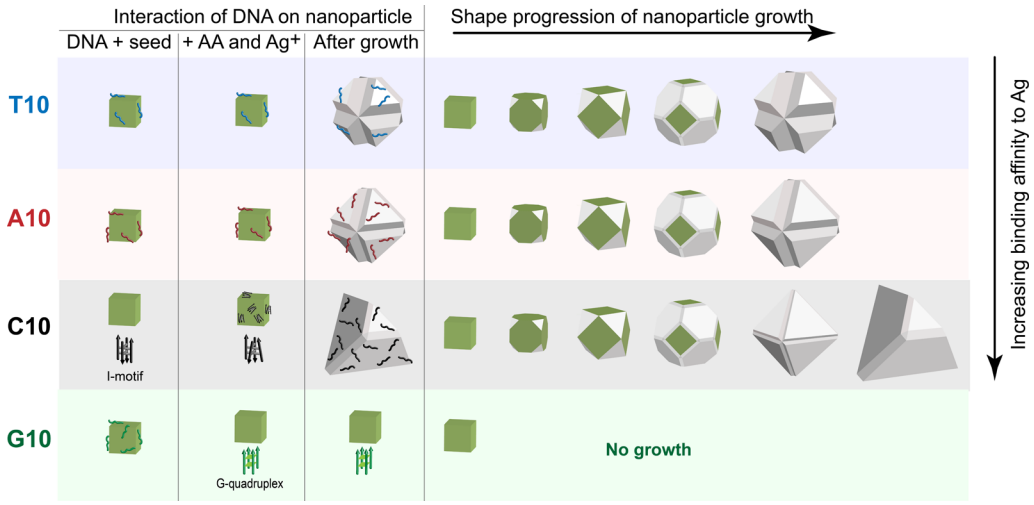

edge length of 74 nm. Figure 3C-a–f shows TEM images and 3D models corresponding to shape evolution from cubic to tetrahedral in the presence of C10. Initial addition of 0.25 μL of 2 mM AgOAc into the solution containing C10 did not change the cubic shape of the seeds (Figure 3C-a). As the total volume of the AgOAc solution was increased to 1.25 μL, Ag cuboctahedra were observed (Figure 3C-b), with addition of 1.25 μL of 2 mM AgOAc resulting in a shape partway between octahedron and cuboctahedron (Figure 3C-c). At a total of 5 μL of AgOAc added, the particles continued to grow into octahedra (Figure 3C-d). Interestingly, the edge truncations of the octahedra formed from oligo-C are much smaller than those observed with oligo-A or -T. Finally, addition to reach a total volume of at least 7.5 μL of AgOAc triggered growth from an octahedron (Figure 3C-e) into an edge-truncated tetrahedron of 100 nm in edge length (Figure 3C-f). Figure S7c (SI) shows the UV–vis spectra of AgNPs depicted in Figure 3C, where it is clearly seen that the major UV peak continuously shifts from 430 nm to 450, 475, and 540 nm, respectively, as the particles evolve into truncated octahedra and tetrahedra.

According to powder X-ray diffraction (XRD) data, the final products of Ag_A10, Ag_T10, and Ag_C10 were dominated by {111} facets, and the peak for (200) planes had all disappeared (SI, Figure S8).[16] This observation suggests that the interactions between DNA (A10, T10, or C10) and silver nanoseeds can slow down the growth rate of Ag {111} facets, and the relatively fast growth rate of Ag {100} results in the disappearance of this facet (Scheme 1).

Despite A, C, and T all preferentially stabilizing the {111} facet, the final morphologies of the nanoparticles are different. The key factor in this difference possibly lies in the different DNA affinity for AgNPs, which has been shown to be in the order of C > G > A > T.[17] To elucidate the role of the DNA affinity in controlling the morphology, we first compared AgNPs growth in the presence of A10 and T10, as the processes of morphological evolution in the presence of A10 and T10 were most comparable. Growth in the presence of A10 took a much longer time (~180 min) than that of T10 (~40 min), consistent with the stronger affinity of A toward AgNPs (Figure 2). Addition of the same amount of silver in the presence of both A10 and T10 resulted in the formation of similar structures, suggesting that the availability of silver is similar but the rate of deposition is different. There are two possible mechanisms for this observed change in rate: the strong DNA binding to the nanoparticle may limit the accessibility of the nanoparticle surface, reducing the rate at which additional silver can deposit on the nanoparticle, or the DNA may bind strongly to free silver ions in solution, thus changing the reduction potential of the Ag^+ reduction reaction and reducing the reduction rate.[6a,18] Both mechanisms are consistent with the observed correlation between the higher binding affinity of A10 to the surface of Ag cubes and the slower deposition rate of Ag^+ ions. On the other hand, T10, which has lower binding affinity for AgNPs, might allow Ag^+ ions easier access to the Ag surface and hence result in a faster growth rate. In both cases the {100} facets on the Ag nanocubes will disappear gradually while the {111} facets become more dominant, resulting in the formation of truncated cubes, and then cuboctahedron-like nanoparticles, and finally truncated octahedral structures. The truncation at the edge of the octahedral structures was observed to be more extensive for T10 than A10, resulting in a particle that is less angled and more spherical. In line with the lower binding affinity of T10, the ability for T10 to stabilize the Ag{111} surface is weaker. The crevices on the edges are likely the result of the DNA being unable to support higher surface energy on the edge of the octahedron. The A10 can stabilize the larger Ag{111} surface and correspondingly result in smaller crevices.

Expanding this explanation toward the Ag_C10 growth process, C10, which has an even higher affinity for AgNPs, is expected to stabilize the Ag{111} facet better than A10 or T10. It was observed that octahedra formed in the intermediate states of Ag_C10 growth have little edge truncation (Figure 3C-d), consistent with our proposed mechanism. Further growth to a tetrahedron from octahedron in the final product suggests a mechanism of growth that is kinetically controlled. That is, the rate of diffusion of the adatoms on the surface is slower than the reduction rate. The migration of the adatoms is limited and cannot be uniformly distributed before further reduction occurs, resulting in four of the eight {111} surfaces on the octahedron being preferentially reduced.[19] Since the kinetic UV data show that the rate of reduction of Ag_C10 is slower than that of Ag_T10, it is likely that the reduction process is fast but the availability of the Ag^+ source is low, resulting in a kinetically trapped reduction.

dx.doi.org/10.1021/ja506150s | J. Am. Chem. Soc. 2014, 136, 15195–15202

Oligomers of C and G are known to form the i-motif[20] and G-quadruplex[21] secondary structures, respectively. The influence of these secondary structures on the kinetics of morphological growth should be considered as well. When single-stranded C10 was dissolved in water, a peak around 290 nm in the CD spectrum was observed (Figure 4a). This CD

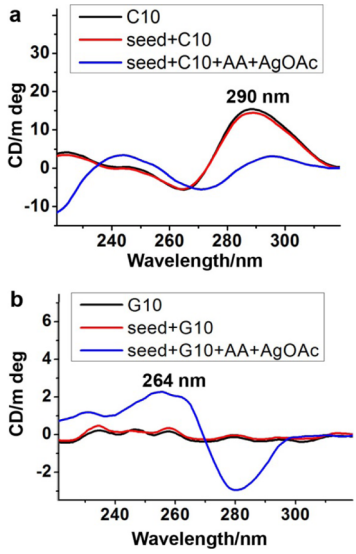

Figure 4. CD spectra of (a) Ag_C10 and (b) Ag_G10 upon addition of AgOAc and AA.

spectrum is typical of i-motif DNA, as reported previously.[22] Addition of the Ag nanocube seed did not cause any changes in the CD spectrum, suggesting that the seed did not perturb the i-motif conformation. Addition of AA and AgOAc resulted in a decrease of the intensity of the 290 nm i-motif peak, suggesting a partial unfolding of the i-motif with reduction of Ag^+ ions. According to a previous DFT calculation,[22] due to the strong binding affinity of oligo-C to Ag^+, the C−H^+−C interaction that stabilizes the i-motif structure can be replaced by a C−Ag^+−C interaction, with a longer distance between the C−C base pairs due to the larger size of Ag^+ compared to H^+. Subsequent reduction of Ag^+ to Ag^0 will then result in destabilization of the i-motif. The partially unfolded C10 might then have enough random coiled region to expose the base for binding to silver cubes, thereby providing access to the seed and allowing Ag to be deposited onto the {100} surface. This process may explain the slow initial growth and absence of the initial blue shift in the UV spectra as observed with both Ag_A10 and Ag_T10. Partial retention of the i-motif may also explain the low availability of silver precursor for reduction, which results in a kinetically driven process, eventually forming tetrahedra.

The case for G10 is interesting as it shows no particular growth from the seeds, despite the affinity of G for silver falling between those of C and A. The secondary structure may provide some insight into the lack of growth. CD spectra of G10 diluted in water alone or in the presence of the Ag nanocube seed displayed few spectral features in the CD spectra (Figure 4b). Addition of reductant and AgOAc resulted in a peak around 264 nm, characteristic of G-quadruplexes. Our observations here are consistent with the reports of previous studies[6b,22] in which G-rich DNA sequences were demonstrated to form G-quadruplexes in the presence of Ag^+. Therefore, unlike the case for C10 where the i-motif is disrupted, the presence of Ag^+ resulted in the formation of G-quadruplex structures and consequent sequestration of the silver precursor. The sequestered silver would not be available for surface deposition on the Ag nanocubes, resulting in the observed lack of size or shape change throughout the growth process.

To test the hypothesis that G-quadruplex formation is the reason that G10 did not exert any influence on the morphological change, we collected the CD spectrum of the supernatant solution after centrifugal separation from the AgNPs. As shown in SI, Figure S9a, the supernatant solution displayed the same CD spectrum of G-quadruplex formation as in the growth solution. The amount of DNA was 99% recovered, suggesting that the majority of the G10 added formed G-quadruplexes with the silver precursor, did not bind to the Ag nanocube seed, and consequently were left in the supernatant. To separate the effects of the secondary structure, we tested AgNP growth in the presence of deoxyguanosine monophosphate (dGMP) that was 10 times the concentration of oligo-G10 so that they would have an equivalent concentration of the G base. In this control, dGMP can bind to the Ag surface through the base but cannot form a G-quadruplex structure to sequester silver ions. As shown in SI, Figure S9b, the cubic seeds changed their shapes after growth mediated by dGMP, suggesting the availability of Ag^+ for reduction. While the ratio of Ag^+ for every G base is 0.4 in our experiment (i.e., 4 Ag^+ per G10 strand), it was reported that the G-quadruplex can be destabilized when the ratio of Ag^+ to G bases is larger than 1.2:1.[6b] As shown in SI, Figure S9c, growth with a 1.2:1 ratio of Ag^+ to G resulted in a morphological change of the Ag nanocubes into truncated tetrahedra. These series of mechanistic insights are summarized in Scheme 1 and demonstrate that binding affinity to the metal surface and metal precursor, location of binding, and DNA secondary structure all play roles in determining the nature and kinetics of the morphological changes of AgNPs.

SERS Properties. A previous report has indicated that Ag colloidal particles in the size range of 80−100 nm are excellent nanomaterials for SERS studies.[23] SI, Figure S10 displays the SERS spectra of 4-methylbenzenethiol[24] adsorbed on the surfaces of these four different nanostructures. Based on the phenyl ring breathing mode at 1079 cm^{-1},[25] the SERS enhancement factors (EFs) were estimated to be $(2.3 \pm 0.1) \times 10^6$, $(1.8 \pm 0.1) \times 10^6$, $(6.0 \pm 0.1) \times 10^5$, and $(5.7 \pm 0.1) \times 10^4$ for Ag_C10, Ag_T10, Ag_A10, and Ag_G10, respectively. The nanoparticles demonstrated shape-dependent SERS enhancement, with Ag_C10 having the highest EF. This EF was found to be reproducible, and the particles did not aggregate after modification of the molecule, as confirmed by the UV−vis absorbance of the particles (SI, Figure S11). Despite Ag_T10 the particles being nearly the same shape and size as a 75 nm octahedron (EF = 2.3×10^5, see SI Figure S10),[2e] the EF value of Ag_T10 was about 8 times higher, suggesting the importance of fine control of the shape, where intraparticle crevices on the truncated Ag_T10 could act as hotspots to enhance the SERS property of the nanoparticle.[26]

Stability and Biorecognition Ability of DNA-Functionalized Ag Nanoparticles. In addition to influencing the morphology of the AgNPs, the DNA molecules that remain on the AgNP surface may still retain their functionality as biorecognition units. To investigate this property, we first probed the stability of the DNA−AgNP complex against

dx.doi.org/10.1021/ja506150s | J. Am. Chem. Soc. 2014, 136, 15195−15202

glutathione (GSH) with AgNPs grown using fluorophore-labeled DNA for quantification. We found that even at an elevated GSH concentration of 10 mM, 95.9% of the A10 remains bound to the particle after 48 h (see SI for detailed procedure). Under the same conditions, AgNPs modified with thiolated oligonucleotides retained only 57.8% of their original DNA (SI, Figure S12). Due to the DNA being embedded in the nanoparticle, this method of growth results in a particle that is stable against displacement by glutathione. The DNA−AgNP conjugates synthesized using monothiolated DNA (SH-DNA) are susceptible to thiol replacement, therefore requiring the use of DNA containing multiple thiol groups to chelate the silver surface.[27] These results demonstrate that our synthesis and controlled reduction method can realize DNA functionalization on AgNP surfaces with high stability while requiring no chemical modifications on the DNA.

To explore the application of these AgNPs in DNA sequence-specific nanoparticle assembly, Ag_A10 particles were incubated with 5 nm gold nanospheres (AuNSs) modified with thiolated complementary DNA T20 (designated as AuNS5nm_S_T20) at a ratio of 1:100 in buffer solution overnight. TEM images were then collected to assess the assembly of the nanoparticles. Figure 5a shows that Ag_A10

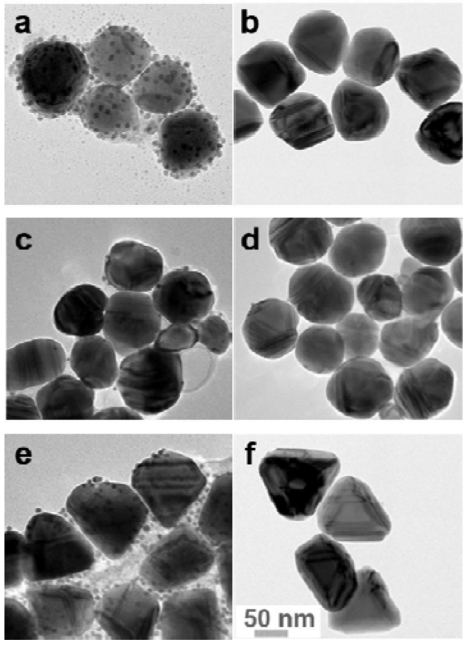

Figure 5. TEM images showing DNA-directed nanoassemblies: (a) Ag_A10 with AuNS5nm_S_T20; (b) Ag_A10 with non-complementary AuNS5nm_S_A20; (c) Ag_T10 with AuNS5nm_S_A20; (d) Ag_T10 with non-complementary AuNS5nm_S_T20; (e) Ag_C10 with AuNS5nm_S_G10; (f) Ag_C10 with non-complementary AuNS5nm_S_C20.

was surrounded by a number of AuNS5nm_S_T20, forming a satellite structure. As a control, when Ag_A10 was incubated with 5 nm AuNSs functionalized with non-complementary DNA, A20 (AuNS5nm_S_A20), no assembly was observed (Figure 5b). Similar results were obtained with Ag_T10 (Figure 5c,d) and Ag_C10 (Figure 5e,f), where AuNS5nm_S_A20 and AuNS5nm_S_G10 were found to attach nanoparticles functionalized with corresponding complementary DNA sequences. Consistent with the lower binding affinity of T for Ag as compared to A or C, fewer AuNSs were observed on the surface of Ag_T10, indicating that fewer T10 strands were attached to Ag_T10 during the synthesis. Unlike nanoparticles functionalized with DNA after the nanoparticles are synthesized,[28] the amount and density of DNA available for hybridization in our system may vary. The growth process will cause an unknown number of the oligonucleotides to become embedded in the nanoparticle during growth. To conduct DNA programmed assembly using more specific sequences than oligo-A or oligo-T, an oligo-A or oligo-T tail can be appended to a specific DNA sequence so that the oligo-A or oligo-T tail can hybridize with oligo-T or oligo-A on the surface of the AgNPs, thus leaving the remaining specific sequence available for further hybridization or additional functionalization.[29] These results confirmed that the DNA molecules are not only able to control the shape of AgNPs but also can retain their molecular recognition properties.

■ CONCLUSIONS

We have demonstrated that DNA can be used to tune AgNP morphology in a sequence-dependent manner, forming truncated tetrahedra with C10, forming differently truncated stellated octahedra with A10 and T10, and retaining the original cubic shape and size with G10. Further kinetic studies using UV−vis, TEM, and CD allowed us to elucidate three important factors in determining the sequence-dependent morphological control, specifically, preferential binding and stabilization of the {111} facets over {100} facets, affinity of DNA toward either Ag nanoparticle or Ag^+ ions in the solution, which affect the growth rates (e.g., A10 vs T10), and the role of secondary structure (e.g., formation of G-quadruplex for G or i-motif for C) in the reaction. These insights have enriched our understanding of biomolecular interactions with nanoparticles and may result in predictive shape control of these bionanomaterials. Finally, the resultant AgNPs with different morphologies displayed shape-dependent properties with SERS EFs ranging from 5.7×10^4 to 2.3×10^6. In addition, the DNA on these AgNPs is more stable than SH-DNA-functionalized AgNPs and retains its biorecognition capabilities, allowing sequence-specific assembly of the nanoparticles.

■ EXPERIMENTAL SECTION

Chemicals and Materials. All oligodeoxyribonucleotides were purchased from Integrated DNA Technologies (Coralville, IA) with standard desalting and without further purification. The DNA concentration was quantified using the absorbance of DNA at 260 nm. MALDI mass spectroscopy was performed on the DNA to confirm sample quality. Ethylene glycol (EG, lot no. G32B27) was obtained from J. T. Baker. Silver trifluoroacetate (CF_3COOAg, ≥99.99%), silver nitrate ($AgNO_3$, 99%), sodium hydrosulfide hydrate ($NaHS{\cdot}xH_2O$), hydrochloric acid (HCl, 37% in water), sodium citrate dehydrate (≥99%), acetone, ascorbic acid (AA), silver acetate (AgOAc), 4-methylbenzenethiol (4-MBT, 98%), and poly(vinylpyrrolidone) (PVP55 with MW ≈ 55 000) were all obtained from Sigma-Aldrich. All aqueous solutions were prepared using deionized (DI) water with a resistivity of 18.2 MΩ·cm. The syntheses of AgNPs were carried out in 35 mL round-bottom flasks (ACE Glass).

Preparation of 40 nm Ag Cube Seeds. Silver cubes were prepared following previously published procedures.[14] In a typical synthesis, 20 mL of EG was added into a 35 mL flask and preheated under magnetic stirring in an oil bath at 150 °C. During the entire process, the flask was capped with a glass stopper except during the addition of reagents. Other reagents dissolved in EG were sequentially added into the flask using a pipet: 250 μL of NaHS solution (3 mM) was first added, and after 2 min, 2 mL of HCl (3 mM) was added,

dx.doi.org/10.1021/ja506150s | J. Am. Chem. Soc. 2014, 136, 15195−15202

followed by 5 mL of PVP55 (20 mg/mL). After another 2 min, 1.5 mL of CF_3COOAg solution (282 mM) was added. The resulting 40 nm cubic Ag seeds were obtained by quenching the reaction with an ice–water bath when the suspension had reached a brown color with a major LSPR peak around 435 nm. After centrifugation and washing once with acetone and twice with DI water, the seeds were redispersed in DI water for further use. The particle size and shape were determined by electron microscopy.

DNA-Mediated Synthesis of the Silver Nanoparticles. The concentration of the purified 40 nm silver nanocubes was measured by UV–vis spectrometry and adjusted to 0.25 absorbance at 430 nm. The particle concentration was 8.834×10^9 particles/mL based on the Ag concentration, as measured using inductively coupled plasma mass spectrometry (ICP-MS), and the particle size and shape were determined by electron microscopy. To 100 μL of this solution was added 5 μL of 1 mM DNA, and this mixture was incubated for 20 min to allow the DNA to adsorb onto the silver nanoseeds. The number of DNA strands added is about 1000 times more than the theoretical amount of DNA needed to cover the surface of each Ag nanocube (~2800 strands/particle assuming the DNA lies flat on the surface of the cube). Excess amounts of DNA were used in order to influence the nanoparticle morphology during growth. Next, 1.5 μL of 70 mM AA was added, and the solution was vortexed. Finally, 10.12 μL of 2 mM AgOAc was introduced to initiate the reduction reaction. A color change was observed, and the reaction was allowed to proceed for 3 h, at which no further color change was observed. The particle size and shape were determined by electron microscopy.

■ ASSOCIATED CONTENT

Supporting Information

Experimental procedures and additional images. This material is available free of charge via the Internet at http://pubs.acs.org.

■ AUTHOR INFORMATION

Corresponding Authors

liwei@tju.edu.cn

yi-lu@illinois.edu

Notes

The authors declare no competing financial interest.

■ ACKNOWLEDGMENTS

The authors thank Lele Li and Hui Wei for insightful discussions and Claire E. McGhee for proofreading of the manuscript. This work has been supported by the China Scholarship Council, the Special Funds for Major State Research Program of China (2012CB720300), and the U.S. National Science Foundation (CMMI-0749028 to Y. L.).

■ REFERENCES

(1) Rycenga, M.; Cobley, C. M.; Zeng, J.; Li, W.; Moran, C. H.; Zhang, Q.; Qin, D.; Xia, Y. *Chem. Rev.* **2011**, *111*, 3669–3712.

(2) (a) Zhang, Q.; Li, W.; Moran, C.; Zeng, J.; Chen, J.; Wen, L.-P.; Xia, Y. *J. Am. Chem. Soc.* **2010**, *132*, 11372–11378. (b) Lei, Y.; Mehmood, F.; Lee, S.; Greeley, J.; Lee, B.; Seifert, S.; Winans, R. E.; Elam, J. W.; Meyer, R. J.; Redfern, P. C.; Teschner, D.; Schlögl, R.; Pellin, M. J.; Curtiss, L. A.; Vajda, S. *Science* **2010**, *328*, 224–228. (c) Guo, W.; Yuan, J.; Wang, E. *Chem. Commun.* **2009**, 3395–3397. (d) Sun, L.; Sun, Y.; Xu, F.; Zhang, Y.; Yang, T.; Guo, C.; Liu, Z.; Li, Z. *Nanotechnology* **2009**, *20*, No. 125502. (e) Zeng, J.; Zheng, Y.; Rycenga, M.; Tao, J.; Li, Z.-Y.; Zhang, Q.; Zhu, Y.; Xia, Y. *J. Am. Chem. Soc.* **2010**, *132*, 8552–8553. (f) Zhang, Q.; Hu, Y.; Guo, S.; Goebl, J.; Yin, Y. *Nano Lett.* **2010**, *10*, 5037–5042. (g) Zhang, Q.; Ge, J.; Pham, T.; Goebl, J.; Hu, Y.; Lu, Z.; Yin, Y. *Angew. Chem., Int. Ed.* **2009**, *48*, 3516–3519. (h) Wei, W.; Li, S.; Qin, L.; Xue, C.; Millstone, J. E.; Xu, X.; Schatz, G. C.; Mirkin, C. A. *Nano Lett.* **2008**, *8*, 3446–3449.

(3) Christopher, P.; Linic, S. *ChemCatChem* **2010**, *2*, 78–83.

(4) Mulvihill, M.; Tao, A.; Benjauthrit, K.; Arnold, J.; Yang, P. *Angew. Chem., Int. Ed.* **2008**, *47*, 6456–6460.

(5) (a) Esumi, K.; Isono, R.; Yoshimura, T. *Langmuir* **2004**, *20*, 237–243. (b) Murugadoss, A.; Chattopadhyay, A. *Nanotechnology* **2008**, *19*, No. 015603. (c) Zhang, H.; Li, X.; Chen, G. *J. Mater. Chem.* **2009**, *19*, 8223–8231. (d) Sun, Y.; Xia, Y. *Science* **2002**, *298*, 2176–2179.

(6) (a) Petty, J. T.; Zheng, J.; Hud, N. V.; Dickson, R. M. *J. Am. Chem. Soc.* **2004**, *126*, 5207–5212. (b) Fu, Y.; Zhang, J.; Chen, X.; Huang, T.; Duan, X.; Li, W.; Wang, J. *J. Phys. Chem. C* **2011**, *115*, 10370–10379. (c) Ritchie, C. M.; Johnsen, K. R.; Kiser, J. R.; Antoku, Y.; Dickson, R. M.; Petty, J. T. *J. Phys. Chem. C* **2007**, *111*, 175–181. (d) Kim, B.-H.; Oh, J.-H.; Han, S. H.; Yun, Y.-J.; Lee, J.-S. *Chem. Mater.* **2012**, *24*, 4424–4433.

(7) Demers, L. M.; Östblom, M.; Zhang, H.; Jang, N.-H.; Liedberg, B.; Mirkin, C. A. *J. Am. Chem. Soc.* **2002**, *124*, 11248–11249.

(8) (a) Braun, E.; Eichen, Y.; Sivan, U.; Ben-Yoseph, G. *Nature* **1998**, *391*, 775–778. (b) Gu, Q.; Cheng, C.; Gonela, R.; Suryanarayanan, S.; Anabathula, S.; Dai, K.; Haynie, D. T. *Nanotechnology* **2006**, *17*, No. R14. (c) Yan, H.; Park, S. H.; Finkelstein, G.; Reif, J. H.; LaBean, T. H. *Science* **2003**, *301*, 1882–1884.

(9) (a) Zhang, J.; Liu, Y.; Ke, Y.; Yan, H. *Nano Lett.* **2006**, *6*, 248–251. (b) Lee, J. H.; Wernette, D. P.; Yigit, M. V.; Liu, J.; Wang, Z.; Lu, Y. *Angew. Chem., Int. Ed.* **2007**, *46*, 9006–9010. (c) Alivisatos, A. P.; Johnsson, K. P.; Peng, X.; Wilson, T. E.; Loweth, C. J.; Bruchez, M. P.; Schultz, P. G. *Nature* **1996**, *382*, 609–611. (d) Zhang, X.; Servos, M. R.; Liu, J. *Chem. Commun.* **2012**, *48*, 10114–10116.

(10) (a) Liu, J.; Cao, Z.; Lu, Y. *Chem. Rev.* **2009**, *109*, 1948–1998. (b) Zhao, W.; Chiuman, W.; Lam, J. C. F.; McManus, S. A.; Chen, W.; Cui, Y.; Pelton, R.; Brook, M. A.; Li, Y. *J. Am. Chem. Soc.* **2008**, *130*, 3610–3618. (c) Lu, Y.; Liu, J. *Acc. Chem. Res.* **2007**, *40*, 315–323. (d) Xu, W.; Xue, X.; Li, T.; Zeng, H.; Liu, X. *Angew. Chem., Int. Ed.* **2009**, *48*, 6849–6852.

(11) (a) Seeman, N. C. *Nature* **2003**, *421*, 427–431. (b) Zhao, W.; Gao, Y.; Kandadai, S. A.; Brook, M. A.; Li, Y. *Angew. Chem., Int. Ed.* **2006**, *45*, 2409–2413. (c) Yan, W.; Xu, L.; Xu, C.; Ma, W.; Kuang, H.; Wang, L.; Kotov, N. A. *J. Am. Chem. Soc.* **2012**, *134*, 15114–15121. (d) Deng, Z.; Tian, Y.; Lee, S.-H.; Ribbe, A. E.; Mao, C. *Angew. Chem., Int. Ed.* **2005**, *44*, 3582–3585. (e) Aldaye, F. A.; Sleiman, H. F. *Angew. Chem., Int. Ed.* **2006**, *45*, 2204–2209. (f) Xu, L.; Ma, W.; Wang, L.; Xu, C.; Kuang, H.; Kotov, N. A. *Chem. Soc. Rev.* **2013**, *42*, 3114–3126. (g) Mirkin, C. A.; Letsinger, R. L.; Mucic, R. C.; Storhoff, J. J. *Nature* **1996**, *382*, 607–609. (h) Tikhomirov, G.; Hoogland, S.; Lee, P. E.; Fischer, A.; Sargent, E. H.; Kelley, S. O. *Nat. Nanotechnol.* **2011**, *6*, 485–490. (i) Xu, L.; Kuang, H.; Xu, C.; Ma, W.; Wang, L.; Kotov, N. A. *J. Am. Chem. Soc.* **2012**, *134*, 1699–1709. (j) Sharma, J.; Chhabra, R.; Cheng, A.; Brownell, J.; Liu, Y.; Yan, H. *Science* **2009**, *323*, 112–116. (k) Storhoff, J. J.; Mirkin, C. A. *Chem. Rev.* **1999**, *99*, 1849–1862. (l) Ma, N.; Sargent, E. H.; Kelley, S. O. *Nat. Nanotechnol.* **2009**, *4*, 121–125. (m) Pal, S.; Deng, Z.; Wang, H.; Zou, S.; Liu, Y.; Yan, H. *J. Am. Chem. Soc.* **2011**, *133*, 17606–17609. (n) Qi, H.; Ghodousi, M.; Du, Y.; Grun, C.; Bae, H.; Yin, P.; Khademhosseini, A. *Nat. Commun.* **2013**, *4*, No. 2275. (o) Tan, S. J.; Campolongo, M. J.; Luo, D.; Cheng, W. *Nat. Nanotechnol.* **2011**, *6*, 268–276. (p) Cheng, W.; Park, N.; Walter, M. T.; Hartman, M. R.; Luo, D. *Nat. Nanotechnol.* **2008**, *3*, 682–690. (q) Pinheiro, A. V.; Han, D.; Shih, W. M.; Yan, H. *Nat. Nanotechnol.* **2011**, *6*, 763–772. (r) Macfarlane, R. J.; Lee, B.; Jones, M. R.; Harris, N.; Schatz, G. C.; Mirkin, C. A. *Science* **2011**, *334*, 204–208. (s) Fu, Y.; Wang, X.; Zhang, J.; Li, W. *Curr. Opin. Biotechnol.* **2014**, *28*, 33–38. (t) Tan, L. H.; Xing, H.; Lu, Y. *Acc. Chem. Res.* **2014**, *47*, 1881–1890. (u) Macfarlane, R. J.; O'Brien, M. N.; Petrosko, S. H.; Mirkin, C. A. *Angew. Chem., Int. Ed.* **2013**, *52*, 5688–5698. (v) Senesi, A. J.; Eichelsdoerfer, D. J.; Macfarlane, R. J.; Jones, M. R.; Auyeung, E.; Lee, B.; Mirkin, C. A. *Angew. Chem., Int. Ed.* **2013**, *52*, 6624–6628.

(12) (a) Cutler, J. I.; Auyeung, E.; Mirkin, C. A. *J. Am. Chem. Soc.* **2012**, *134*, 1376–1391. (b) Lee, J. H.; Yigit, M. V.; Mazumdar, D.; Lu, Y. *Adv. Drug Delivery Rev.* **2010**, *62*, 592–605. (c) Xing, H.; Wong, N. Y.; Xiang, Y.; Lu, Y. *Curr. Opin. Chem. Biol.* **2012**, *16*, 429–435.

(13) (a) Wang, Z.; Zhang, J.; Ekman, J. M.; Kenis, P. J. A.; Lu, Y. *Nano Lett.* **2010**, *10*, 1886–1891. (b) Wang, Z.; Tang, L.; Tan, L. H.;

Li, J.; Lu, Y. *Angew. Chem., Int. Ed.* **2012**, *51*, 9078−9082. (c) Richards, C. I.; Choi, S.; Hsiang, J.-C.; Antoku, Y.; Vosch, T.; Bongiorno, A.; Tzeng, Y.-L.; Dickson, R. M. *J. Am. Chem. Soc.* **2008**, *130*, 5038−5039. (d) Wang, Q.; Liu, Y.; Ke, Y.; Yan, H. *Angew. Chem., Int. Ed.* **2007**, *47*, 316−319.
(14) Xia, X.; Zeng, J.; Oetjen, L. K.; Li, Q.; Xia, Y. *J. Am. Chem. Soc.* **2012**, *134*, 1793−1801.
(15) Siekkinen, A. R.; McLellan, J. M.; Chen, J.; Xia, Y. *Chem. Phys. Lett.* **2006**, *432*, 491−496.
(16) Temgire, M. K.; Joshi, S. S. *Radiat. Phys. Chem.* **2004**, *71*, 1039−1044.
(17) Basu, S.; Jana, S.; Pande, S.; Pal, T. *J. Colloid Interface Sci.* **2008**, *321*, 288−293.
(18) (a) Yamane, T.; Davidson, N. *Biochim. Biophys. Acta* **1962**, *55*, 609−621. (b) Wu, S.; Zhao, H.; Ju, H.; Shi, C.; Zhao, J. *Electrochem. Commun.* **2006**, *8*, 1197−1203.
(19) Wang, Y.; Xie, S.; Liu, J.; Park, J.; Huang, C. Z.; Xia, Y. *Nano Lett.* **2013**, *13*, 2276−2281.
(20) (a) Guéron, M.; Leroy, J.-L. *Curr. Opin. Struct. Biol.* **2000**, *10*, 326−331. (b) Gehring, K.; Leroy, J.-L.; Gueron, M. *Nature* **1993**, *363*, 561−565.
(21) (a) Keniry, M. A. *Biopolymers* **2000**, *56*, 123−146. (b) Gellert, M.; Lipsett, M. N.; Davies, D. R. *Proc. Natl. Acad. Sci. U.S.A.* **1962**, *48*, 2013−2018.
(22) Wu, J.; Fu, Y.; He, Z.; Han, Y.; Zheng, L.; Zhang, J.; Li, W. *J. Phys. Chem. B* **2012**, *116*, 1655−1665.
(23) Emory, S. R.; Nie, S. *J. Phys. Chem. B* **1998**, *102*, 493−497.
(24) Li, W.; Camargo, P. H. C.; Lu, X.; Xia, Y. *Nano Lett.* **2009**, *9*, 485−490.
(25) (a) Osawa, M.; Matsuda, N.; Yoshii, K.; Uchida, I. *J. Phys. Chem.* **1994**, *98*, 12702−12707. (b) Sauer, G.; Brehm, G.; Schneider, S. *J. Raman Spectrosc.* **2004**, *35*, 568−576.
(26) Mulvihill, M. J.; Ling, X. Y.; Henzie, J.; Yang, P. *J. Am. Chem. Soc.* **2010**, *132*, 268−274.
(27) (a) Dougan, J. A.; Karlsson, C.; Smith, W. E.; Graham, D. *Nucleic Acids Res.* **2007**, *35*, 3668−3675. (b) Pal, S.; Sharma, J.; Yan, H.; Liu, Y. *Chem. Commun.* **2009**, 6059−6061. (c) Thompson, D. G.; Enright, A.; Faulds, K.; Smith, W. E.; Graham, D. *Anal. Chem.* **2008**, *80*, 2805−2810. (d) Lee, J.-S.; Lytton-Jean, A. K. R.; Hurst, S. J.; Mirkin, C. A. *Nano Lett.* **2007**, *7*, 2112−2115.
(28) Storhoff, J. J.; Elghanian, R.; Mirkin, C. A.; Letsinger, R. L. *Langmuir* **2002**, *18*, 6666−6670.
(29) Li, L.-L.; Wu, P.; Hwang, K.; Lu, Y. *J. Am. Chem. Soc.* **2013**, *135*, 2411−2414.